Scientific Reports

https://doi.org/10.1038/s41598-026-56745-6

Article in Press

Role of polyacrylonitrile fiber diameter and aspect ratio on mechanical performance and pore structure of cementitious mortars

Received: 17 February 2026

Accepted: 2 June 2026

Published online: 07 June 2026

Cite this article as: Culgatay V.G. & Ozturk M. Role of polyacrylonitrile fiber diameter and aspect ratio on mechanical performance and pore structure of cementitious mortars. *Sci Rep* (2026). https://doi.org/10.1038/s41598-026-56745-6

Vedat Goktug Culgatay & Murat Ozturk

We are providing an unedited version of this manuscript to give early access to its findings. Before final publication, the manuscript will undergo further editing. Please note there may be errors present which affect the content, and all legal disclaimers apply.

If this paper is publishing under a Transparent Peer Review model then Peer Review reports will publish with the final article.

ARTICLE IN PRESS

© The Author(s) 2026. **Open Access** This article is licensed under a Creative Commons Attribution-NonCommercial-NoDerivatives 4.0 International License, which permits any non-commercial use, sharing, distribution and reproduction in any medium or format, as long as you give appropriate credit to the original author(s) and the source, provide a link to the Creative Commons licence, and indicate if you modified the licensed material. You do not have permission under this licence to share adapted material derived from this article or parts of it. The images or other third party material in this article are included in the article's Creative Commons licence, unless indicated otherwise in a credit line to the material. If material is not included in the article's Creative Commons licence and your intended use is not permitted by statutory regulation or exceeds the permitted use, you will need to obtain permission directly from the copyright holder. To view a copy of this licence, visit http://creativecommons.org/licenses/by-nc-nd/4.0/.

ARTICLE IN PRESS

Role of Polyacrylonitrile Fiber Diameter and Aspect Ratio on Mechanical Performance and Pore Structure of Cementitious Mortars

Vedat Goktug CULGATAY[1] Murat OZTURK[1]*

[1] Smart Materials Laboratory, Bursa Uludag University, Engineering Faculty, Civil Engineering, Bursa 16059, Türkiye

*Corresponding author. ORCID ID: 0000-0003-3389-4883; Email: muratozturk@uludag.edu.tr

Abstract

This study investigates how the geometric parameters of synthetic microfibers—specifically fiber diameter and resulting aspect ratio—govern the transition between crack-bridging–dominated reinforcement and matrix-densification–driven strengthening in cementitious mortars. Polyacrylonitrile (PAN) fibers with identical length (6 mm) but three distinct diameters (≈15, 35, and 40 μm) are incorporated at volume fractions ranging from 0.2% to 0.6%, enabling isolation of aspect ratio effects under controlled conditions. Rather than treating fiber reinforcement as a purely mechanical addition, the results demonstrate that below a critical fiber diameter, PAN fibers act as an active microstructural modifier. Finer fibers with higher aspect ratios promote a shift in the governing strengthening mechanism—from conventional crack-bridging to simultaneous pore refinement and enhanced stress transfer at the fiber–matrix interface. This transition is evidenced by a coupled improvement in compressive and flexural strength, accompanied by a pronounced reduction in harmful capillary and macropores, as confirmed by mercury intrusion porosimetry (MIP)and scanning electron microscopy (SEM). In contrast, mortars reinforced with coarser PAN fibers exhibit behavior consistent with classical fiber reinforcement models, where mechanical performance remains largely insensitive to fiber content and microstructural refinement is limited. These findings indicate that fiber

ARTICLE IN PRESS

geometry defines not only reinforcement efficiency but also the dominant physical mechanism by which fibers interact with the cementitious matrix.

Keywords: PAN fiber; Fiber geometry; Cementitious mortar; Mechanical properties; Microstructure

1. Introduction

Cement-based composites, which are primarily produced by mixing aggregate, cement, water, and chemical or mineral admixtures, are among the most widely used construction materials worldwide [1]. These materials are readily available, easily castable, and generally exhibit high compressive strength and satisfactory durability [2]. However, cementitious composites such as concrete and mortar are intrinsically weak under tensile stresses and tend to crack in a brittle manner [3]. For this reason, significant research efforts are devoted to improving the tensile-related performance of cement-based composites [4–11], among which fiber reinforcement is one of the most effective and widely adopted approaches.

Fibers are commonly incorporated into cementitious composites to restrain crack initiation and propagation by transferring stresses across cracks formed due to shrinkage or mechanical loading [12,13]. Microfibers are mainly employed to mitigate early-age shrinkage cracking [14], whereas macrofibers are generally used to enhance post-cracking performance under higher stress levels [15]. Through these mechanisms, fiber reinforcement is known to improve toughness [16], ductility [17], and energy absorption capacity [18]. However, the efficiency of fibers is strongly governed by parameters such as fiber length, diameter, volume fraction, orientation, dispersion, and fiber–matrix interfacial properties [19–22]. In particular, the fiber aspect ratio (length-to-diameter ratio) plays a critical role in determining crack-bridging efficiency and load transfer capability [23–26].

ARTICLE IN PRESS

Beyond mechanical loading, cement-based composites may also experience deterioration and premature service failure due to aggressive environmental conditions. Fiber reinforcement has been reported to limit crack width development, thereby slowing down damage accumulation and improving durability. This contribution becomes especially important under conditions such as shrinkage [27], freeze–thaw cycles [28], acid attack [29], sulfate attack [30], and exposure to elevated temperatures [31], where cracking accelerates the ingress of harmful agents and intensifies degradation mechanisms.

In practical applications, steel [32], glass [33], natural [34], and synthetic fibers [35] are widely used. Steel fibers can significantly improve flexural strength and post-cracking resistance; however, corrosion susceptibility may raise concerns regarding long-term durability [36]. Glass fibers are limited by their brittle nature and insufficient alkali resistance unless specially treated [37]. Natural fibers may provide moderate improvements in flexural tensile behavior, yet their relatively low strength and durability-related variability restrict their widespread use [38]. In contrast, synthetic fibers are frequently preferred due to their low cost, chemical stability, and adequate mechanical performance. Synthetic fibers such as nylon [39], polypropylene [40], polyolefin [40], acrylic [41], carbon [42], polyvinyl alcohol [43], polyethylene terephthalate [44], and polyacrylonitrile (PAN) fibers [45] have been reported in the literature.

Although synthetic fibers have been extensively investigated, studies focusing specifically on PAN fibers in cementitious mortars remain scarce, particularly with respect to the combined influence of fiber diameter, length, and resulting aspect ratio on both mechanical and durability performance. PAN fibers produced via the electrospinning technique are characterized by small and controllable fiber diameters, high specific surface area, and favorable interfacial interaction potential, which are expected to influence

ARTICLE IN PRESS

dispersion quality and crack-bridging behavior [46]. The effect of PAN fiber diameter on the geometric efficiency of stress transfer and on the resulting mechanical and pore-structural behavior of cementitious mortars has not yet been systematically clarified. The present study addresses this specific gap by isolating fiber-diameter-controlled effects under otherwise identical mix-design conditions.

Accordingly, the novelty of this study lies in the systematic use of PAN fibers with three different diameters (15, 35, and 40 μm) and a fixed length (6 mm), introduced into mortar mixtures at volume fractions of 0.2%, 0.4%, and 0.6%. This design enables a clear investigation of the influence of fiber aspect ratio on the performance of PAN fiber-reinforced mortars. The experimental program encompasses the assessment of fresh-state behavior via flow diameter measurements, hardened-state properties through compressive and flexural strength tests, and microstructural characteristics by evaluating apparent porosity, scanning electron microscopy (SEM), and mercury intrusion porosimetry (MIP) for pore size distribution analysis.

2. Materials and method

Mortar mixtures are prepared using Portland cement CEM I 42.5R, calcareous fine aggregate, potable water, and PAN fibers. The cement is supplied by Bursa Cement (Bursa, Türkiye) and has a specific gravity of 3.10. Calcareous crushed stone aggregate with a maximum particle size of 4 mm and a specific gravity of 2.65 is used as fine aggregate. Potable tap water is employed as mixing water in all mixtures.

PAN fibers supplied by AKSA Akrilik Kimya Sanayi A.Ş. (Yalova, Türkiye) are used as the reinforcing material. The fibers are cut into nominal lengths of 6 mm prior to mixing. For each fiber length, three different nominal fiber diameters (≈15 μm, ≈35 μm, and ≈40 μm) are considered. Fiber diameters are determined by measuring ten randomly selected fibers from SEM, and

ARTICLE IN PRESS

average values are calculated. The physical and mechanical properties of the PAN fibers provided by the manufacturer (AKSA Akrilik Kimya Sanayi A.Ş.) are presented in Table 1, and representative optical images of the fibers are shown in Figure 1.

Table 1. The physical and mechanical properties of the polyacrylonitrile fibers

Product	Dtex	Fiber Diameter (μm)	Cut Length (mm)	Fiber Density (g/cm³)	Tensile Strength (cN/Tex)	Elongation at Break (%)	Young's Modulus (cN/T)
PAN-A	1.7	≈15	6	1.17 – 1.18	≥ 50	≥ 16	300
PAN-B	8.7	≈35	6	1.17 – 1.18	≥ 35	≥ 10	350
PAN-C	17	≈40	6	1.17 – 1.18	≥ 30	≥ 10	400

ARTICLE IN PRESS

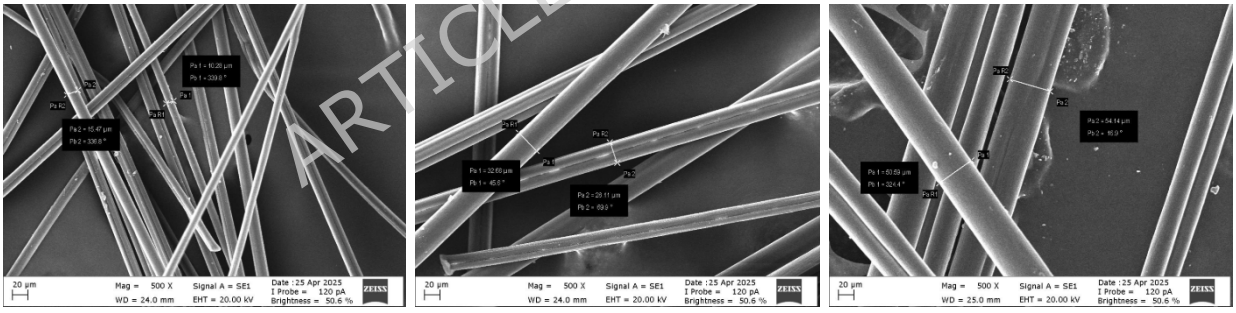


Figure 1. Scanning electron microscopy pictures of polyacrylonitrile fibers a) PAN-A, b) PAN-B and c) PAN-C

A reference mortar mixture is prepared using a cement-to-aggregate-to-water mass ratio of 1:2.75:0.485. Based on this reference mixture, PAN fiber-reinforced mortars are produced by incorporating fibers at three different fiber volume fractions (Vf): 0.2%, 0.4%, and 0.6%.

ARTICLE IN PRESS

The fiber volume fraction is defined as the ratio of the total fiber volume to the total composite volume and is expressed as a percentage. The selected volume fractions are chosen to evaluate the influence of fiber content on mechanical and durability performance while maintaining acceptable workability and uniform fiber dispersion. Due to the relatively low density and small diameter of PAN fibers compared to steel fibers, lower fiber volume fractions are sufficient to activate crack-bridging and stress-transfer mechanisms. Preliminary mixing trials indicate that fiber volume fractions exceeding 0.6% cause fiber agglomeration and severe reductions in workability; therefore, the maximum fiber volume fraction is limited to 0.6%.

For each fiber volume fraction, constant fiber length (6 mm,) and three fiber diameters (15 µm, 35 µm, and 40 µm) are investigated. Accordingly, the combined effects of fiber volume fraction and fiber aspect ratio (length-to-diameter ratio, L/D) on the mechanical and durability performance of cementitious mortars are systematically examined. It should be noted that in the experimental design, fiber length is held constant at 6 mm; therefore, fiber diameter constitutes the only independently controlled geometric variable, and aspect ratio (L/D) is a mathematically derived parameter. The detailed mix design parameters and fiber geometric properties are presented in Table 2. The mix-ID convention is defined as PAN-(fiber length in mm)-(fiber diameter in µm)-(fiber volume fraction in %); for example, PAN-6-15-0.2 designates a mortar reinforced with 6 mm long, ≈15 µm diameter PAN fibers at a volume fraction of 0.2%.

Table 2. Mix design, fiber volume fractions, and geometric properties of polyacrylonitrile fiber-reinforced cementitious mortars

ARTICLE IN PRESS

Mix ID	Cement	Aggregate	Water	Fiber volume fraction Vf (%)	Fiber length-L (mm)	Fiber diameter-D (μm)	Aspect ratio (L/D)
REF	1.00	2.75	0.485	0.0	–	–	–
PAN-6-15-0.2	1.00	2.75	0.485	0.2	6	15	4000
PAN-6-35-0.2	1.00	2.75	0.485	0.2	6	35	1710
PAN-6-40-0.2	1.00	2.75	0.485	0.2	6	40	1500
PAN-6-15-0.4	1.00	2.75	0.485	0.4	6	15	4000
PAN-6-35-0.4	1.00	2.75	0.485	0.4	6	35	1710
PAN-6-40-0.4	1.00	2.75	0.485	0.4	6	40	1500
PAN-6-15-0.6	1.00	2.75	0.485	0.6	6	15	4000
PAN-6-35-0.6	1.00	2.75	0.485	0.6	6	35	1710

ARTICLE IN PRESS

ARTICLE IN PRESS

Mix ID	Cement	Aggregate	Water	Fiber volume fraction Vf (%)	Fiber length-L (mm)	Fiber diameter-D (μm)	Aspect ratio (L/D)
PAN-6-40-0.6	1.00	2.75	0.485	0.6	6	40	1500

Dry materials consisting of cement, aggregate, and PAN fibers are initially mixed using a mechanical Hobart-type mixer to ensure uniform fiber dispersion. Mixing water is then added gradually, and mixing is continued until a homogeneous fresh mortar is obtained. Fresh mortar is cast into oiled steel molds with dimensions of 40 × 40 × 160 mm^3 for flexural testing and 50 × 50 × 50 mm^3 for compressive testing. Specimens are stored in the molds for 24 hours under laboratory conditions, then demolded and cured in a water tank at ambient temperature for 28 days.

The flow behavior of fresh mortars is characterized through the flow table test, following the procedure outlined in ASTM C1437 [47]. A standard truncated cone mold, measuring 100 mm in base diameter, 70 mm at the top, and 50 mm in height, is utilized for shaping the mortar prior to testing. The mold is positioned centrally on the flow table surface and filled with mortar in two successive layers. Each layer is compacted by delivering 15 uniform tamping blows using a standard rod, ensuring consistent layer density. After filling, the mold is gently removed in a vertical direction to avoid disturbing the material. Subsequently, the flow table is operated by applying 25 drops from a specified height within a 15-second period, as prescribed in the standard. Upon completion of the drops, the maximum spread diameters are measured in two perpendicular directions. The mean of these measurements is taken as the flow value. For each mixture, at least three tests are carried out, and the results are expressed as the average flow diameter.

ARTICLE IN PRESS

Flexural tensile strength is determined using a three-point bending test in accordance with ASTM C348 [48]. Prismatic specimens with dimensions of 40 × 40 × 160 mm are placed on two steel supports with a span length of 100 mm. Load is applied at the mid-span using a servo-controlled universal testing machine at a constant displacement rate in accordance with standard practice. Loading is continued until failure occurs. Test results are reported as the average of three specimens for each mixture.

Compressive strength tests are conducted on cubic specimens with dimensions of 50 × 50 × 50 mm in accordance with ASTM C109 [49]. Specimens are loaded between steel platens of a servo-controlled testing machine with a capacity of 500 kN. Load is applied at a constant rate until specimen failure occurs. Six specimens are tested for each mixture, and the average compressive strength value is reported.

The apparent porosity of the mortar specimens is determined on 28-day cured samples incorporating PAN fibers. At the time of testing, all specimens are kept in a saturated-surface-dry (SSD) condition. Each specimen is weighed in this state and then placed in a ventilated oven at 50 °C. The drying process is continued until no further weight loss is observed, indicating that a constant dry mass has been reached. A relatively low drying temperature is selected in order to avoid thermal microcracking that may occur at elevated temperatures. After stabilization, the oven-dried specimens are weighed again. Apparent porosity (%) is calculated using the following equation in accordance with the principles of ASTM C642 [50]:

$$\text{Apparent porosity (\%)} = \frac{W_{ssd} - W_{dry}}{W_{dry}} \times 100 \quad (1)$$

where W_{ssd} denotes the saturated-surface-dry weight and W_{dry} represents the oven-dry weight of the specimen. For each mixture, a minimum of six specimens is tested, and the average value is reported as the final result.

ARTICLE IN PRESS

SEM is used to investigate the microstructural characteristics of the cementitious composites and to examine the interaction between the cement matrix and PAN fibers. In addition, the influence of fiber incorporation on the internal structure and fiber–matrix bonding behavior of the composites is evaluated. SEM analyses are carried out using a ZEISS EVO 40 scanning electron microscope. Prior to imaging, specimens are vacuum-dried and coated with a thin layer of gold to ensure electrical conductivity. SEM observations are performed at various magnification levels. The microstructural features of cementitious composites with different fiber contents, fiber lengths, and fiber diameters are examined using SEM images obtained from 28-day-old specimens.

Pore structure analysis is performed using MIP with a PoreMaster33 instrument. Approximately 1 g of representative fragments is collected from the central region of specimens after compressive strength testing to minimize surface-related damage and edge effects. Prior to testing, the samples are dried in a vacuum oven at 60 °C for 24 hours to remove residual moisture without altering the pore structure. The measurements are conducted sequentially under low-pressure and high-pressure intrusion stages, allowing mercury to penetrate pores over a wide size range. The applied pressure is gradually increased from the low-pressure mode up to approximately 33,000 psi, enabling the determination of pore size distribution and cumulative intrusion volume based on the Washburn equation [51].

ARTICLE IN PRESS

3. Results and discussion

3.1. Flow table

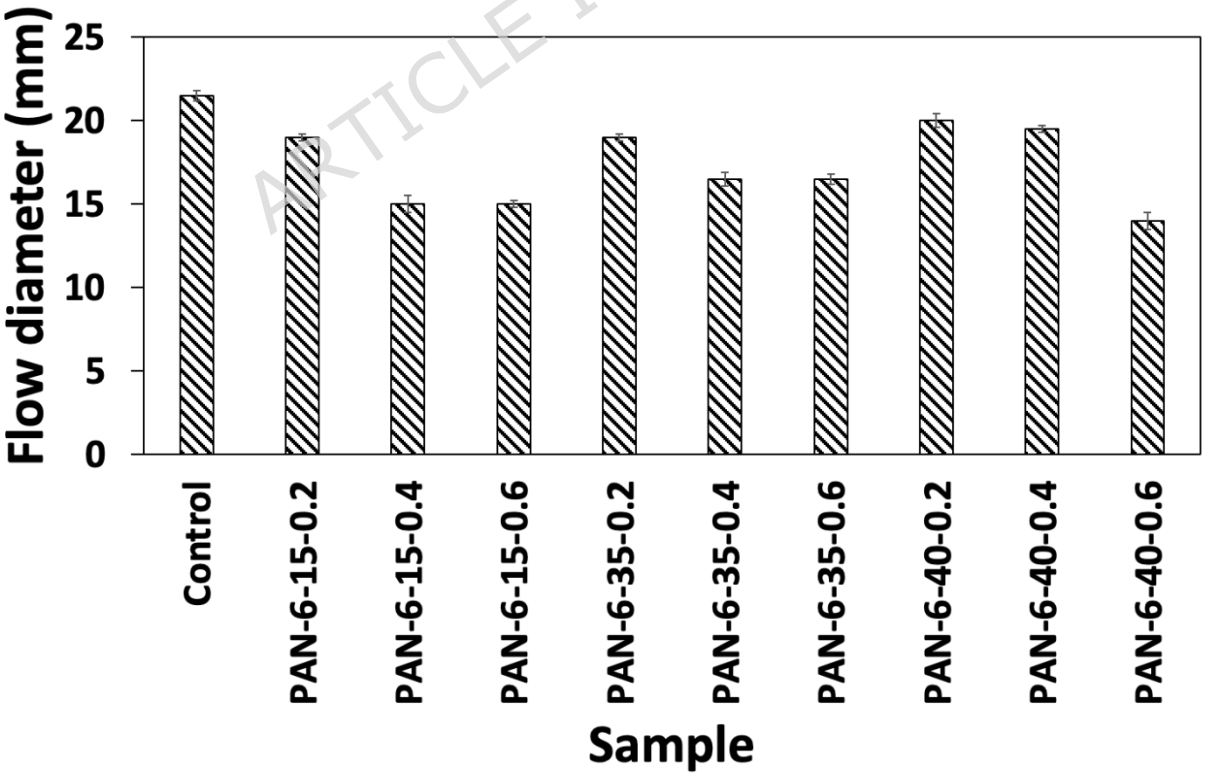
The flow table test results of PAN fiber reinforced mortar samples are presented in Figure 2. The control mixture exhibits the highest flow diameter (21.5 ± 0.3 cm), indicating high workability in the absence of PAN fibers. All fiber-reinforced mixtures show reduced flow values, and this reduction

ARTICLE IN PRESS

becomes more evident with increasing fiber content and decreasing fiber diameter.

For mixtures containing 15 μm PAN fibers, the flow diameter decreases from 19.0 ± 0.2 cm (PAN-6-15-0.2) to 15.0 ± 0.2 cm (PAN-6-15-0.6) as the fiber volume fraction increases from 0.2% to 0.6%. A similar decreasing trend is observed for mixtures with 35 μm PAN fibers, with flow values of 19.0 ± 0.2 cm, 16.5 ± 0.4 cm, and 16.5 ± 0.3 cm for 0.2%, 0.4%, and 0.6% fiber contents, respectively. In mixtures incorporating 40 μm PAN fibers, the spread diameter varies between 20.0 ± 0.4 cm (PAN-6-40-0.2) and 14.0 ± 0.5 cm (PAN-6-40-0.6), where the lowest value corresponds to the combination of highest fiber length and content. The overall trend shows that increasing PAN fiber content and length tends to reduce mortar flowability [52]. The flow diameter generally decreases as more fibers are added and as they become longer or finer in diameter, indicating the sensitivity of fresh mortar rheology to PAN fiber characteristics.

ARTICLE IN PRESS



ARTICLE IN PRESS

Figure 2. Flow diameter results of the mortars including polyacrylonitrile fibers

3.2. Flexural tensile strength

Figure 3 presents the 28-day flexural tensile strength values of mortars incorporating PAN fibers with varying volume fractions and fiber diameters. The flexural strength of the control mixture without fiber reinforcement is measured as 8.30 MPa. In fiber-reinforced mixtures, both increases and decreases in flexural strength are observed depending on the fiber characteristics. A general increasing trend is identified in mixtures containing fine PAN fibers (≈15 µm), especially as the fiber volume fraction increases. In this group, PAN-6-15-0.2, PAN-6-15-0.4, and PAN-6-15-0.6 exhibit flexural strengths of 8.64 MPa, 8.82 MPa, and 8.94 MPa, corresponding to increases of approximately 4.1%, 6.3%, and 7.7%, respectively, compared to the control.

For mixtures containing medium fiber diameters (≈35 µm), more variable results are obtained. A decrease of approximately 5.9% is recorded in PAN-6-35-0.2, with a measured strength of 7.81 MPa. When the fiber volume fraction is increased to 0.4% (PAN-6-35-0.4), a slight improvement is observed, yielding 8.39 MPa, which corresponds to a 1.1% increase. At the highest fiber volume fraction (PAN-6-35-0.6), the strength reaches 8.72 MPa, indicating a 5.1% improvement over the control.

In contrast, mixtures incorporating coarser fibers (≈40 µm) generally exhibit lower flexural strength values compared to the control. The specimens PAN-6-40-0.2 and PAN-6-40-0.4 attain strengths of 7.32 MPa and 7.34 MPa, reflecting reductions of 11.8% and 11.5%, respectively. PAN-6-40-0.6, although at a higher fiber content, shows a flexural strength of 7.79 MPa, which remains 6.1% lower than the reference mixture.

In general, it is observed that the effect of PAN fiber addition on flexural tensile strength is highly dependent on both fiber diameter and content. An

ARTICLE IN PRESS

increasing trend is consistently observed in mixtures with fine fibers and higher volume fractions, whereas a decline in performance is generally recorded when thicker fibers are used, particularly at lower contents. This improvement is mainly associated with the crack-bridging action of PAN fibers, which enhances the flexural performance of the mortar specimens [53].

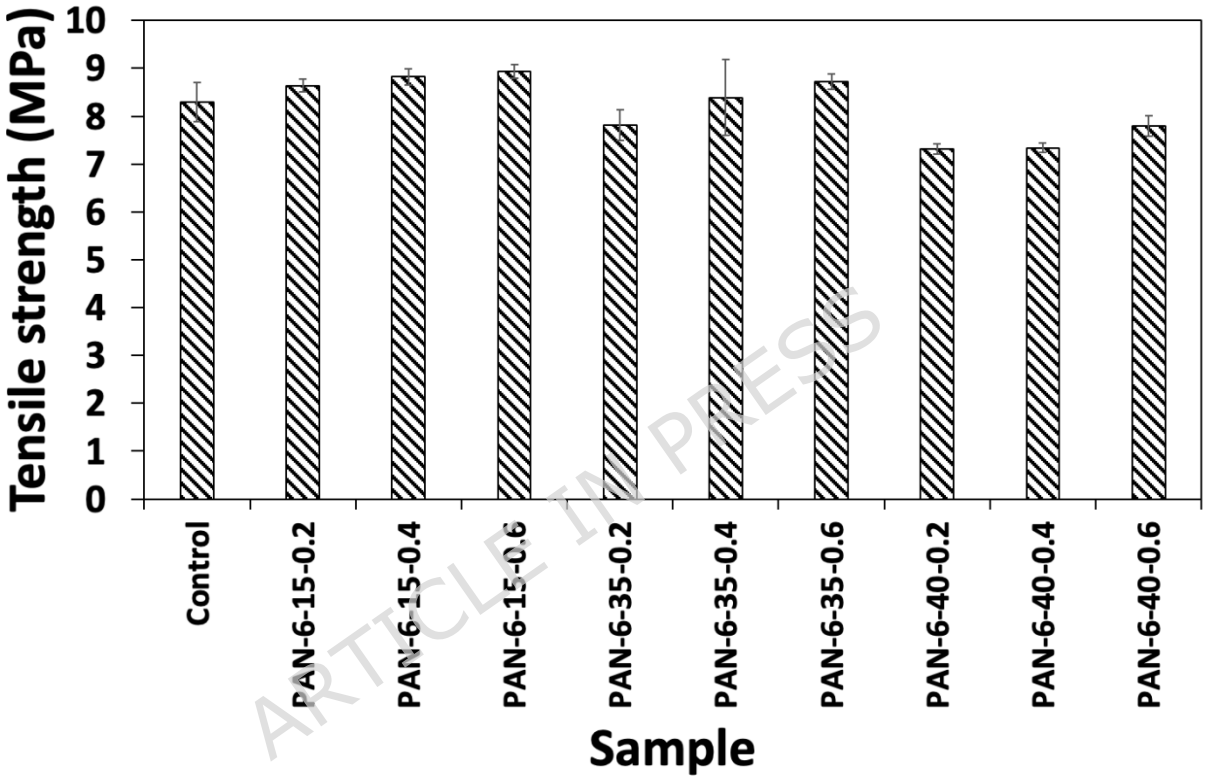


Figure 3. The 28-day flexural tensile strength values of mortars incorporating PAN fibers

3.3. Compressive strength

The 28-day compressive strength values of mortar mixtures incorporating PAN fibers are presented in Figure 4. The reference mixture reaches a compressive strength of 54.01 MPa. Mixtures containing medium (≈35 µm) and coarse (≈40 µm) PAN fibers generally exhibit compressive strengths comparable to the control. For example, PAN-6-35-0.4 and PAN-6-35-0.6

ARTICLE IN PRESS

attain values of 53.55 MPa and 53.48 MPa, representing negligible decreases of 0.9% and 1.0%, respectively. In mixtures with 40 μm PAN fibers, compressive strength remains largely stable or slightly improved. PAN-6-40-0.2 and PAN-6-40-0.4 show small increases of 3.7% and 4.1%, while PAN-6-40-0.6 reaches 62.36 MPa, marking a notable 15.4% increase over the control. This non-linear response suggests a threshold-type behavior, in which a critical fiber number density must be reached before coarse fibers can effectively contribute to load transfer, whereas finer fibers — owing to their higher number density at equivalent volume fractions — surpass this threshold even at lower contents.

On the other hand, a more pronounced and consistent improvement is observed in mixtures incorporating 15 μm PAN fibers. With increasing fiber content, compressive strength rises progressively, from 54.51 MPa in PAN-6-15-0.2 (+0.9%) to 59.87 MPa in PAN-6-15-0.4 (+10.9%), reaching 71.67 MPa in PAN-6-15-0.6, which corresponds to a substantial 32.7% increase.

Furthermore, the flexural strength values of these mixtures follow a similar trend, particularly for specimens containing fine PAN fibers, indicating that improvements in compressive performance are accompanied by enhanced tensile capacity. These observations suggest that, in addition to their role in crack bridging, finely dispersed PAN fibers may also function as microfillers, contributing to overall matrix densification. Owing to their uniform dispersion within the cementitious matrix, these fibers may contribute to a more homogeneous and isotropic internal structure [54].

Although synthetic fibers are generally considered to have limited influence on compressive behavior [55], the present findings indicate that fiber geometry—particularly small diameter and adequate volume—can influence not only tensile performance but also the densification of the mortar structure through porosity reduction.

ARTICLE IN PRESS

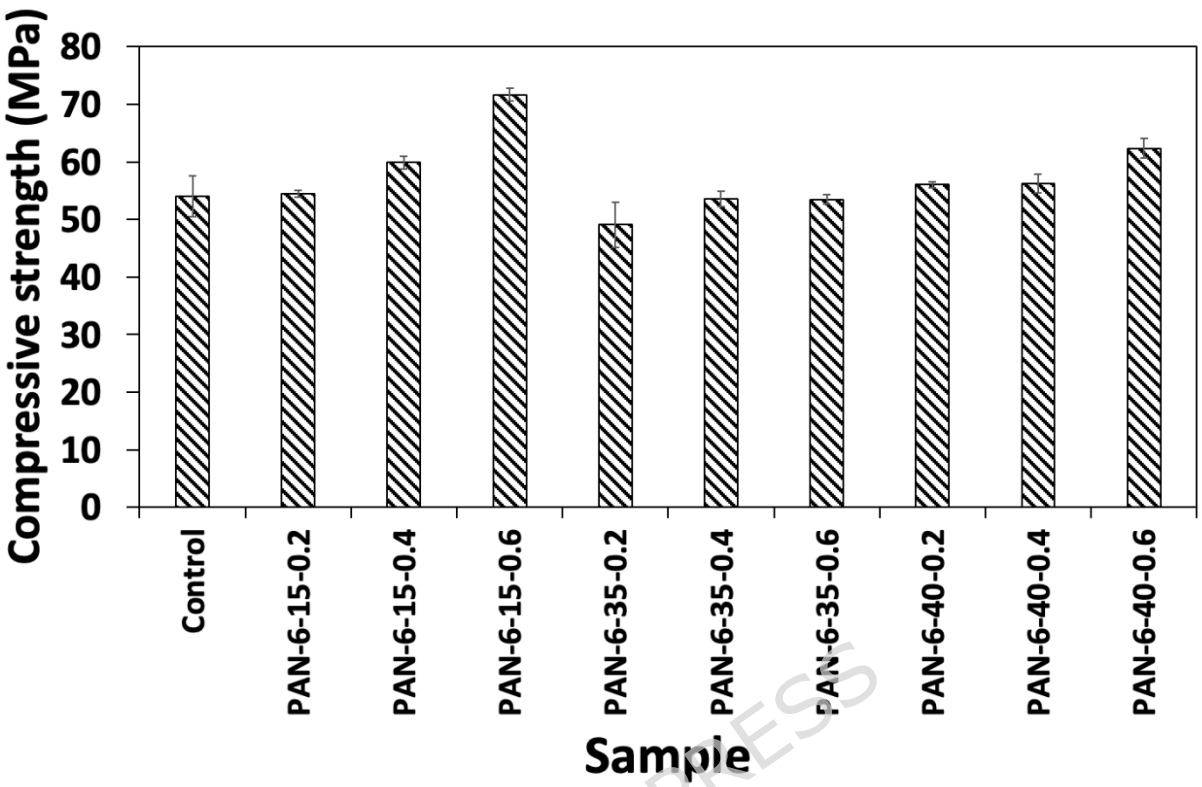


Figure 4. The 28-day compressive strength values of mortars incorporating polyacrylonitrile fibers

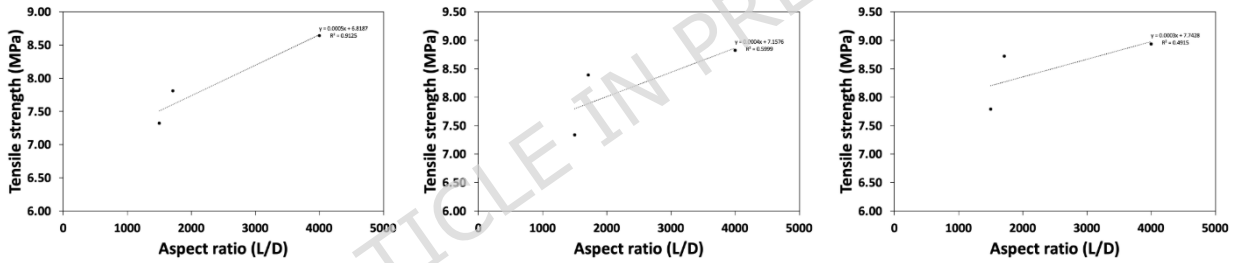
3.4. Influence fiber aspect ratio on mechanical performance

The influence of PAN fiber aspect ratio on mechanical performance at a constant fiber length of 6 mm is illustrated in Figures 5 (a, b, and c) and 6 (a, b, and c). A clear positive trend is observed between aspect ratio and both compressive and flexural tensile strengths. Specifically, mortars containing 15 µm PAN fibers (L/D ≈ 4000) exhibit consistently higher strength values compared to those with 35 µm fibers (L/D ≈ 1710) at identical fiber volume fractions. For instance, at 0.2 vol%, compressive strength increases from 49.10 MPa to 54.51 MPa (+11%), while flexural tensile strength rises from 7.81 MPa to 8.64 MPa (+10.6%) when the aspect ratio increases from 1710 to 4000. Similarly, at 0.4 vol%, the compressive strength improves from 53.55 MPa to 59.87 MPa (+11.8%), and flexural tensile strength increases from 8.39 MPa to 8.82 MPa (+5.1%). These results indicate that a higher fiber

ARTICLE IN PRESS

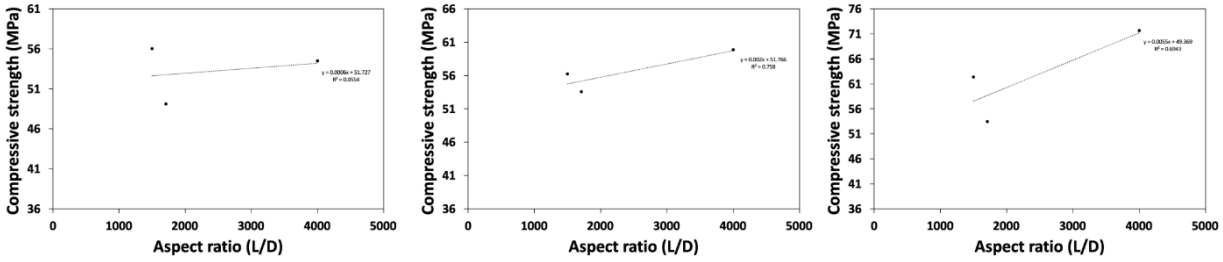
aspect ratio enhances the reinforcing efficiency of PAN fibers in cementitious matrices.

This improvement can be attributed to multiple mechanisms. Finer PAN fibers, due to their smaller diameter, provide a significantly higher specific surface area per unit volume compared to coarser ones. As the fiber surface area increases, the potential for fiber–matrix interfacial bonding also increases. This stronger bond promotes more effective stress transfer under load and facilitates crack-bridging mechanisms, especially in tensile loading scenarios [56]. In addition, the denser distribution of thinner fibers within the matrix may enhance their ability to fill microvoids and disrupt capillary porosity, leading to a more compact and homogenous internal structure. As a result, both strength and durability parameters benefit from the synergistic effects of improved matrix densification and fiber bridging.



(a) (b) (c)

Figure 5. Aspect ratio vs Tensile strength of mortar including a) 0.2 vol% polyacrylonitrile -fiber, b) 0.4 vol% polyacrylonitrile -fiber and c) 0.6 vol% polyacrylonitrile -fiber



(a) (b) (c)

ARTICLE IN PRESS

Figure 6. Aspect ratio vs Compressive strength of mortar including a) 0.2 vol% polyacrylonitrile -fiber, b) 0.4 vol% polyacrylonitrile -fiber and c) 0.6 vol% polyacrylonitrile -fiber

3.5. Apparent porosity

The apparent porosity results of the mortar mixtures are presented in Figure 7. The control mixture exhibits a porosity of 7.17 ± 0.40%. All PAN fiber-reinforced mixtures display lower porosity values compared to the control, indicating that the inclusion of PAN fibers contributes to a denser matrix by reducing internal voids.

For mixtures incorporating 15 µm PAN fibers, porosity values decrease with increasing fiber content: 6.17 ± 1.37% for PAN-6-15-0.2, 5.89 ± 0.71% for PAN-6-15-0.4, and 5.85 ± 0.39% for PAN-6-15-0.6. A similar trend is observed in mixtures containing 35 µm fibers, with porosity values of 6.28 ± 0.21%, 6.02 ± 0.30%, and 5.93 ± 0.27% for 0.2%, 0.4%, and 0.6% volume fractions, respectively. For the mixtures with 40 µm PAN fibers, porosity also tends to decrease as the fiber content increases, with values of 6.61 ± 0.50%, 6.21 ± 0.61%, and 5.89 ± 0.43%.

These results suggest that higher PAN fiber contents, particularly when finer fibers are used, are effective in reducing the apparent porosity of cementitious mortars. This trend may be attributed to the ability of thin and well-dispersed PAN fibers to fill microvoids and improve the packing density of the composite, thereby reducing overall pore volume.

ARTICLE IN PRESS

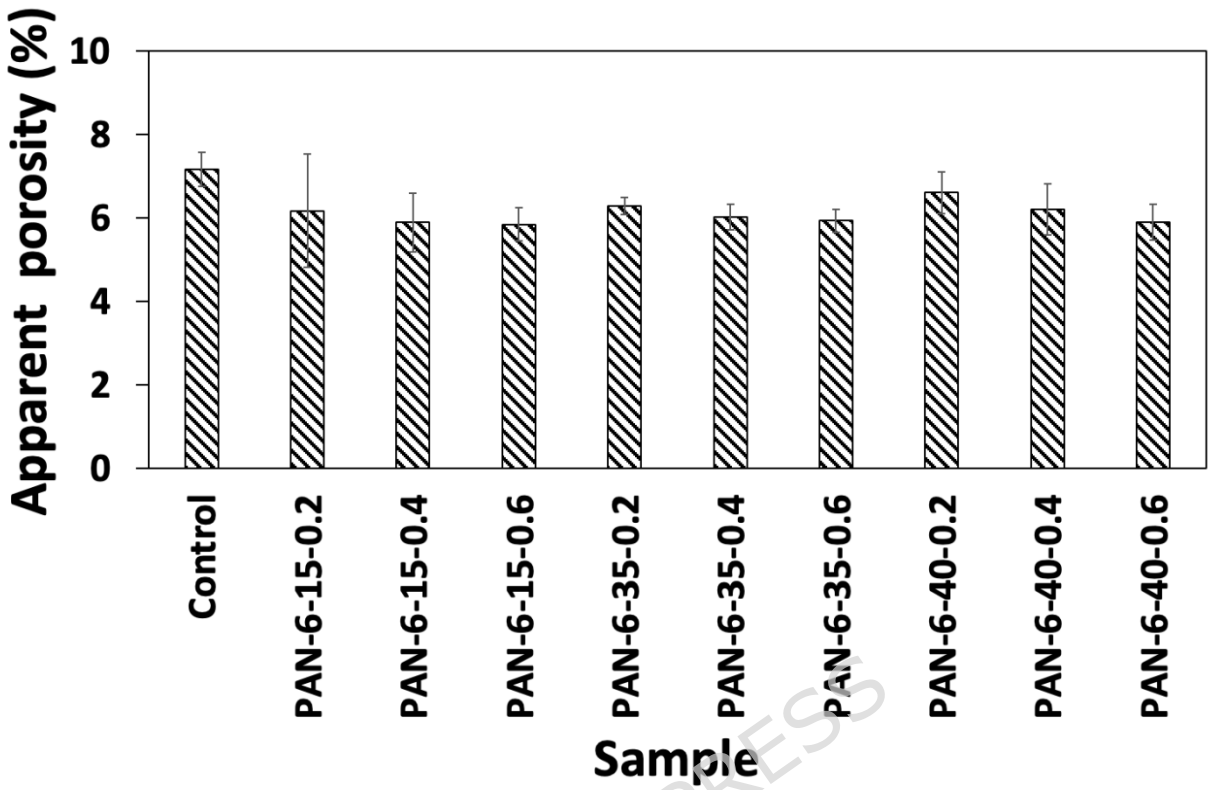


Figure 7. The apparent porosity results of the mortar mixtures

3.6. Scanning electron microscopy

Representative SEM images of the fractured surfaces of selected mortar specimens incorporating PAN fibers—PAN-6-15-0.6, PAN-6-35-0.6, and PAN-6-40-0.6—are presented in Figure 8, illustrating the fiber–matrix interaction and post-fracture behavior at 28 days.

In the case of PAN-6-15-0.6, a strong physical bond between the PAN fibers and the cementitious matrix is clearly observed. The embedded fiber appears well anchored, and the fiber itself is noticeably thinned and torn, indicating that tensile loads have been effectively transferred from the matrix to the fiber. The ductile failure mode exhibited—characterized by elongation and rupture—suggests high energy absorption capacity and confirms the fiber's contribution to both tensile and compressive performance. This observation aligns with the highest flexural tensile strength (8.94 MPa) and compressive

ARTICLE IN PRESS

strength (71.67 ± 0.39 MPa) recorded among all mixtures, as well as the lowest porosity (5.85 ± 0.39%), indicating a well-integrated and dense microstructure.

In contrast, the image corresponding to PAN-6-35-0.6 reveals a more brittle fracture mechanism. The PAN fibers appear broken with clean fracture surfaces, rather than tapered or necked ends, suggesting that the load transfer may have reached the fiber's failure limit without sufficient elongation or pull-out. Although this mixture still exhibits relatively good flexural and compressive performance, the energy dissipation capacity appears lower compared to the 15 μm fiber group. The observed fracture mode supports the moderately high but less exceptional mechanical values.

For PAN-6-40-0.6, PAN fibers are also observed to be fractured; however, unlike the previous cases, noticeable interfacial voids remain at the fiber–matrix boundaries. These gaps may indicate weak interfacial bonding or possible fiber debonding during loading, which could impair stress transfer and reduce the reinforcement efficiency. This microstructural evidence corresponds with the relatively lower flexural tensile strength (7.79 MPa) and a moderate compressive strength (62.36 ± 0.43 MPa) compared to PAN-12-15-0.6. Despite being the same volume fraction (0.6%), the inferior mechanical performance may be attributed to reduced interfacial adhesion and less effective crack-bridging behavior.

The diameter-dependent transition between fiber rupture and fiber pull-out observed in Figure 8 can be rationalized within the classical Aveston–Cooper–Kelly framework, in which the dominant failure mode shifts from pull-out to rupture when the embedded fiber length exceeds the critical embedded length. Within the same 6 mm fiber length and matrix system, the substantially larger specific surface area and stronger interfacial bond developed by the fine 15 μm fibers reduce critical embedded length below the available embedded length, favoring the necking-rupture failure mode visible in the PAN-6-15-0.6 micrograph and corresponding to high energy

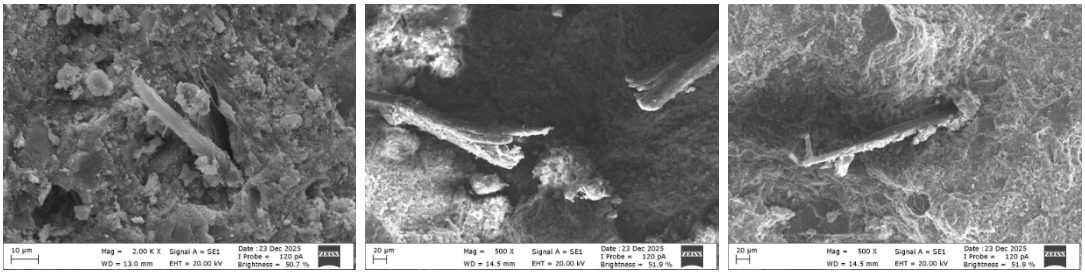
ARTICLE IN PRESS

absorption. Increasing the fiber diameter to ≈35 μm raises critical embedded length through both the direct fiber diameter scaling and the concomitant reduction of interfacial bonding area, producing the clean fracture surfaces observed in PAN-6-35-0.6. For the coarsest 40 μm fibers, the further increase of critical embedded length above the available embedded length combined with the lower fiber–matrix bond favors fiber debonding and pull-out, which is consistent with the interfacial voids observed at the fiber boundary in PAN-6-40-0.6. It is acknowledged that two-dimensional SEM observations represent a sub-sample of the three-dimensional fiber network; complementary three-dimensional imaging methods such as X-ray micro-computed tomography are identified as a priority direction for future investigation.

These microstructural findings emphasize that the efficiency of PAN fibers in enhancing mechanical performance is closely tied to their interaction with the surrounding matrix. Particularly, fiber–matrix adhesion quality, the presence or absence of interfacial voids, and the nature of fiber failure (e.g., rupture vs. debonding) appear to govern the extent of load transfer and crack control. The fine PAN fibers demonstrate a more integrated and cohesive behavior within the matrix, likely promoting better mechanical interlocking and reduced porosity. In contrast, coarser fibers exhibit signs of interfacial detachment or brittle failure, which may undermine their reinforcing potential.

Although direct quantitative dispersion mapping (e.g., optical microscopy or X-ray computed tomography) was not performed in the present study, the relatively low coefficient of variation in the mechanical test results across replicate specimens, together with the SEM evidence of individually anchored fibers in Figure 8, indirectly supports the assumption of acceptable dispersion quality. A dedicated quantitative dispersion analysis is identified as a key direction for future investigation.

ARTICLE IN PRESS



(a) (b) (c)

Figure 8. Scanning electron microscopy images of the fractured surfaces of mortar specimens incorporating polyacrylonitrile fibers

a) PAN-6-15-0.6, b) PAN-6-35-0.6, and c) PAN-6-40-0.6

3.7. Mercury intrusion porosimetry

The pore characteristics of selected mortar specimens—Control, PAN-6-15-0.6, PAN-6-35-0.6, and PAN-6-40-0.6—were assessed using mercury intrusion porosimetry (MIP) after 28 days of curing. These samples are selected based on their fiber type and content, representing the highest PAN fiber volume fraction (0.6 vol%) within each diameter group and exhibiting distinct compressive strength behaviors. The differential intrusion and cumulative pore volume distributions are presented in Figure 9(a) and Figure 9(b), respectively. Furthermore, Figure 9(c) illustrates the volumetric distribution of pore sizes categorized into defined ranges.

The characteristics of cementitious composites are primarily controlled by the relative proportions of pores at different scales, rather than by porosity alone [57]. The analysis revealed that most of the pore volume across all samples is concentrated between 10 nm and 1000 nm, covering both mesoporous (10–100 nm) and capillary (100–1000 nm) domains. According to conventional classifications, pores are divided into four categories: gel pores (<10 nm), mesopores (10–100 nm), capillary pores (100–1000 nm), and macropores (>1000 nm). Among these, pores exceeding 100 nm are typically

ARTICLE IN PRESS

regarded as detrimental to mechanical performance due to their negative effect on matrix integrity and stress distribution[58,59] .

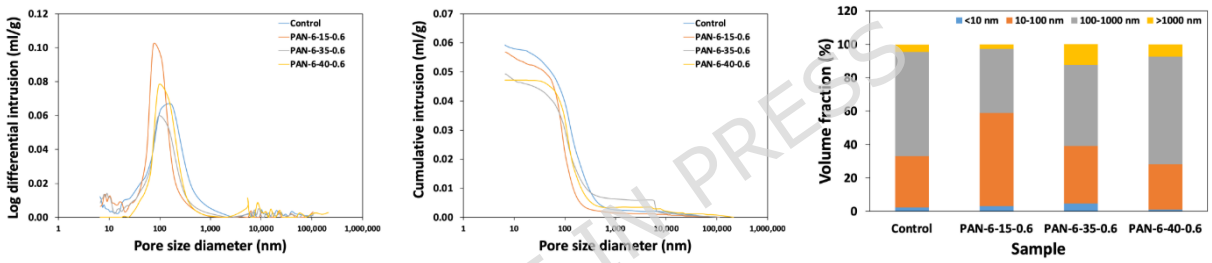
In terms of quantitative results, PAN-6-15-0.6 displays the most favorable pore refinement, with 3.20% gel pores, 55.60% mesopores, 38.40% capillary pores, and a minimal macropore volume of 2.70%. This structure implies enhanced matrix densification, which may be attributed to the high surface area and uniform dispersion of the fine PAN fibers, promoting better packing and limiting void formation. In contrast, PAN-6-35-0.6 contains 12.50% macropores, indicating poorer microstructural development and potentially explaining its relatively lower compressive strength. PAN-6-40-0.6 also shows a considerable share of macropores (7.40%) and a high capillary pore content (64.40%), suggesting a less compact internal matrix.

These microstructural trends closely align with the mechanical performance of the specimens. The mixture incorporating the finest PAN fibers demonstrated the most refined pore structure, particularly characterized by reduced macroporosity, which corresponded with the highest levels of both compressive and flexural tensile strength. This suggests that finer fibers enhance the matrix densification by limiting the formation of larger pores and improving particle packing within the cementitious matrix. In comparison, the specimen reinforced with medium-diameter fibers exhibited the most prominent presence of large pores and the lowest mechanical performance, highlighting the detrimental influence of macropores on strength development. The sample containing the coarsest PAN fibers displayed behavior similar to the medium-fiber specimen, both in terms of pore structure and mechanical response. This similarity indicates that increasing fiber diameter beyond a certain point does not significantly alter the pore structure or performance benefits.

The reduction of capillary and macropore volume in fine-fiber mixtures may not be ascribed to direct geometric infill by the fibers, since PAN fibers of ≈15 μm diameter are two to three orders of magnitude larger than typical

ARTICLE IN PRESS

capillary pores (≈0.1–1 µm). The observed pore-structure refinement is more rigorously interpreted as the convergence of three coupled mechanisms: (i) modification of fresh-state particle packing, in which finely dispersed fibers reorganize the cement–aggregate–water configuration and inhibit the formation of large entrapped air voids during mixing and compaction; (ii) refinement of the interfacial transition zone surrounding each fiber, where dense calcium silicate hydrate (C–S–H) develops preferentially along the high specific surface area of fine fibers; and (iii) heterogeneous nucleation, in which the polar nitrile (–C≡N) groups of PAN promote local precipitation of hydration products, densifying the matrix immediately adjacent to each fiber and disrupting the spatial continuity of large capillary channels.



(a) (b) (c)

Figure 9. Mercury intrusion porosimetry analsis results of the polyacrylonitrile fiber mortars a) differential pore size distribution curve, b) cumulative pore size distribution curve and c) volumetric distribution of pore sizes

4. Conclusion

The findings of this study confirm that PAN fiber geometry, particularly fiber diameter and aspect ratio, plays a critical role in determining the fresh, mechanical, and microstructural behavior of cementitious mortars. Finer PAN fibers (≈15 µm) with higher aspect ratios demonstrated superior performance in terms of compressive and flexural strength, primarily due to improved fiber–matrix interaction and internal pore structure refinement. SEM and MIP analyses revealed that these fibers contributed to better

ARTICLE IN PRESS

dispersion, stronger interfacial bonding, and significant reductions in harmful macroporosity. In contrast, mortars with coarser PAN fibers exhibited more brittle fracture modes and higher residual porosity, resulting in lower mechanical performance.

Given these findings, PAN fiber-reinforced mortars show strong potential for use in repair mortars, precast components, architectural panels, and thin-section elements where enhanced crack control, dimensional stability, and durability are required. Their low density and chemical resistance make them particularly suitable for lightweight and corrosion-sensitive environments.

However, certain limitations of the present work should be acknowledged. The study focused on a single fiber length (6 mm) and a limited range of volume fractions (up to 0.6%), primarily to avoid dispersion and workability issues. In addition, while the mechanical and microstructural properties were comprehensively evaluated, long-term durability aspects—such as shrinkage, creep, freeze–thaw resistance, or chloride permeability—were not within the scope of this investigation. Also, fiber dispersion quality and orientation were not quantitatively assessed, which may influence mechanical variability.

Future studies could explore broader ranges of fiber length, hybrid fiber systems, and functional surface modifications to further improve the compatibility and performance of PAN fibers in cement matrices. Additionally, rheological characterization, advanced imaging (e.g., X-ray CT), and durability-focused testing under aggressive environmental conditions would provide a more complete understanding of PAN-reinforced systems. Investigating the economic and environmental implications of PAN fiber use could also support their broader adoption in sustainable construction practices.

Data Availability Statement

Data will be available on reosanable request.

ARTICLE IN PRESS

Competing interests

The authors declare that they have no competing interests.

Acknowledgments

This study was supported by Bursa Uludag University Research Projects Coordination Office under the Grant Number FGA-2025-2027. The authors thank to BUU BAP Unit for their support.

References

[1] H. Li, Y. Du, J. Yang, D. Lei, N. Zhang, L. Wang, Synergistic nano-reinforcement in strain-hardening cement composites: Unlocking the potential of graphene oxide/carbon nanotube hybrids, Composites Part A: Applied Science and Manufacturing 201 (2026) 109409. https://doi.org/10.1016/j.compositesa.2025.109409.
[2] Z. Li, X. Zhou, H. Ma, D. Hou, Advanced Concrete Technology, John Wiley & Sons, 2022.
[3] S. Zhang, B. Han, H. Xie, M. An, S. Lyu, S. Zhang, B. Han, H. Xie, M. An, S. Lyu, Brittleness of Concrete under Different Curing Conditions, Materials 14 (2021). https://doi.org/10.3390/ma14247865.
[4] J. Fu, V. Sarfarazi, H. Haeri, Z. Wang, M. Fatehi Marji, Improving the tensile strength of reinforced concrete: evaluating the impact of different fiber additives through numerical and experimental analysis, Computational Particle Mechanics 12 (2025) 775–792. https://doi.org/10.1007/s40571-024-00839-3.
[5] Z. Chen, X. Wang, K. Jiang, X. Zhao, X. Liu, Z. Wu, The splitting tensile strength and impact resistance of concrete reinforced with hybrid BFRP minibars and micro fibers, Journal of Building Engineering 88 (2024) 109188. https://doi.org/10.1016/j.jobe.2024.109188.
[6] H. Zhu, Z. Fu, Y. Wang, N. Zhang, Study on splitting tensile strength of interface between the full lightweight ceramsite concrete and ordinary concrete, Case Studies in Construction Materials 18 (2023) e01829. https://doi.org/10.1016/j.cscm.2023.e01829.
[7] J. Pan, W. Zhong, J. Wang, C. Zhang, Size effect on dynamic splitting tensile strength of concrete: Mesoscale modeling, Cement and Concrete Composites 128 (2022) 104435. https://doi.org/10.1016/j.cemconcomp.2022.104435.
[8] S.S. Solanke, P.Y. Pawade, H. Ali Khan, An experimental study on tensile as well as flexural strength of concrete by using sugarcane baggase ash & steel fiber, Materials Today: Proceedings 60 (2022) 627–637. https://doi.org/10.1016/j.matpr.2022.02.129.

ARTICLE IN PRESS

[9] T. Kiran, N. Anand, M.E. Mathews, B. Kanagaraj, A.D. Andrushia, E. Lubloy, J. G, Investigation on improving the residual mechanical properties of reinforcement steel and bond strength of concrete exposed to elevated temperature, Case Studies in Construction Materials 16 (2022) e01128. https://doi.org/10.1016/j.cscm.2022.e01128.
[10] P. Men, X. Wang, D. Liu, Z. Zhang, Q. Zhang, Y. Lu, On use of polyvinylpyrrolidone to modify polyethylene fibers for improving tensile properties of high strength ECC, Construction and Building Materials 417 (2024) 135354. https://doi.org/10.1016/j.conbuildmat.2024.135354.
[11] H. Wang, X. He, M. Zhou, B. Wei, W. Wu, G. Zhou, J. He, A study on the tensile fracture behavior of polypropylene fiber reinforced concrete based on a microscale model, Construction and Building Materials 417 (2024) 135291. https://doi.org/10.1016/j.conbuildmat.2024.135291.
[12] J. Qiu, Y. Li, F. Xu, X. Hu, Y. Xiao, Strain induced crack initiation and the subsequent crack propagation of fiber-reinforced resin composites, Composites Part A: Applied Science and Manufacturing 155 (2022) 106836. https://doi.org/10.1016/j.compositesa.2022.106836.
[13] H. Li, W. Xu, C. Zhang, D.-Y. Yoo, N. Banthia, L. Wang, J. Yang, D.C.W. Tsang, The road ahead in interfacial engineering of recycled fiber composites, Composites Part B: Engineering 317 (2026) 113613. https://doi.org/10.1016/j.compositesb.2026.113613.
[14] M. Saqib, M.F. Javed, M.I. Khan, Investigation of drying shrinkage response in fibrillated microfiber reinforced preplaced concrete: experimental analysis and prediction models, Innov. Infrastruct. Solut. 9 (2024) 397. https://doi.org/10.1007/s41062-024-01718-9.
[15] H. Yuan, X.H. Fu, Y.C. Fan, B. Fu, Q.Q. Zou, Flexural performance of layered macro fiber reinforced concrete beams, Construction and Building Materials 357 (2022) 129314. https://doi.org/10.1016/j.conbuildmat.2022.129314.
[16] E.A.H. Alwesabi, B.H. Abu Bakar, I.M.H. Alshaikh, A.A. Abadel, H. Alghamdi, M. Wasim, An experimental study of compressive toughness of Steel–Polypropylene hybrid Fibre-Reinforced concrete, Structures 37 (2022) 379–388. https://doi.org/10.1016/j.istruc.2022.01.025.
[17] X. Zhao, F. Zhou, W. Wang, D. Kong, J. Liu, H. Wu, Dynamic compressive behavior of polyethylene fiber reinforced high strength and high ductility concrete over wide ranges of strain rate, Journal of Building Engineering 80 (2023) 107953. https://doi.org/10.1016/j.jobe.2023.107953.
[18] G. Liu, D. Li, Analysis of synergistic effect of bending energy absorption capacity of fiber reinforced concrete based on fiber distribution characteristic, Construction and Building Materials 447 (2024) 138098. https://doi.org/10.1016/j.conbuildmat.2024.138098.
[19] A. Aksoy, E. Yigit, A.B. Caglayan, M. Ozturk, Interpretation and analysis of scattering in steel fiber alignment in concrete: The H alpha decomposition method using fully polarized B-scan ground penetrating

ARTICLE IN PRESS

radar (GPR) image data, Journal of Building Engineering 105 (2025) 112472. https://doi.org/10.1016/j.jobe.2025.112472.
[20] A.B. Çağlayan, M. Öztürk, A. Aksoy, E. Yigit, Fully polarimetric GPR and H-alpha decomposition for scattering-based characterization of fiber-reinforced concrete, Measurement 256 (2025) 118503. https://doi.org/10.1016/j.measurement.2025.118503.
[21] O. Akgol, E. Unal, M. Bağmancı, M. Karaaslan, U.K. Sevim, M. Öztürk, A. Bhadauria, A Nondestructive Method for Determining Fiber Content and Fiber Ratio in Concretes Using a Metamaterial Sensor Based on a V-Shaped Resonator, J. Electron. Mater. 48 (2019) 2469–2481. https://doi.org/10.1007/s11664-019-06937-w.
[22] M. Ozturk, U.K. Sevim, O. Akgol, M. Karaaslan, E. Unal, An electromagnetic non-destructive approach to determine dispersion and orientation of fiber reinforced concretes, Measurement 138 (2019) 356–367. https://doi.org/10.1016/j.measurement.2019.01.039.
[23] L. Li, C. Yang, W. Shu, H. Xu, Y. Zeng, Z. Zhu, Z. Zou, S. Jia, Study on the deformation and cracking characteristics of bamboo fiber reinforced concrete anti-slide pile considering the aspect ratio, fiber dosage and its coupling effect with rebars, Engineering Structures 294 (2023) 116750. https://doi.org/10.1016/j.engstruct.2023.116750.
[24] S. Bankir, M. Bikce, Experimental investigation and statistical evaluation of the effects of steel fiber aspect ratio and fiber rate on static and dynamic mechanical properties of concrete, Construction and Building Materials 414 (2024) 135064. https://doi.org/10.1016/j.conbuildmat.2024.135064.
[25] G. Laxmi, S.G. Patil, Effect of fiber types, shape, aspect ratio and volume fraction on properties of geopolymer concrete – A review, Materials Today: Proceedings 65 (2022) 1086–1094. https://doi.org/10.1016/j.matpr.2022.04.157.
[26] O. Yavuz Bayraktar, G. Kaplan, J. Shi, A. Benli, B. Bodur, M. Turkoglu, The effect of steel fiber aspect-ratio and content on the fresh, flexural, and mechanical performance of concrete made with recycled fine aggregate, Construction and Building Materials 368 (2023) 130497. https://doi.org/10.1016/j.conbuildmat.2023.130497.
[27] K. Aghaee, K.H. Khayat, Design and performance of fiber-reinforced shrinkage compensating eco-friendly concrete, Construction and Building Materials 408 (2023) 133803. https://doi.org/10.1016/j.conbuildmat.2023.133803.
[28] J. Zhang, Y. Guan, C. Fan, G. Cao, J. Liu, Experimental and theoretical investigations on the damage evolution of the basalt fiber reinforced concrete under freeze-thaw cycles, Construction and Building Materials 422 (2024) 135703. https://doi.org/10.1016/j.conbuildmat.2024.135703.
[29] J. Xiao, J. Liu, R. Liang, L. Liu, J. Feng, Z. He, X. Chen, H. Jiang, Durability assessment of UHPC with varying steel fiber contents under sulfuric acid Attack: Macro-Micro characterization, Engineering Failure

ARTICLE IN PRESS

Analysis (2026) 110523. https://doi.org/10.1016/j.engfailanal.2025.110523.
[30] N. Liang, J. Mao, R. Yan, X. Liu, X. Zhou, The damage evolution behavior of polypropylene fiber reinforced concrete subjected to sulfate attack based on acoustic emission, Front. Struct. Civ. Eng. 16 (2022) 316–328. https://doi.org/10.1007/s11709-022-0810-8.
[31] L. Lu, F. Han, S. Wu, Y. Qin, G. Yuan, J.-H. Doh, Experimental study on durability of basalt fiber concrete after elevated temperature, Structural Concrete 23 (2022) 682–693. https://doi.org/10.1002/suco.202000746.
[32] J. Ahmad, Z. Zhou, A.F. Deifalla, Steel Fiber Reinforced Self-Compacting Concrete: A Comprehensive Review, Int J Concr Struct Mater 17 (2023) 51. https://doi.org/10.1186/s40069-023-00602-7.
[33] Ch. Devi, D.S. Vijayan, R. Nagalingam, S. Arvindan, A review of the implementations of glass fiber in concrete technology, Materials Today: Proceedings 62 (2022) 2010–2015. https://doi.org/10.1016/j.matpr.2022.02.293.
[34] L. Chen, Z. Chen, Z. Xie, L. Wei, J. Hua, L. Huang, P.-S. Yap, Recent developments on natural fiber concrete: A review of properties, sustainability, applications, barriers, and opportunities, Developments in the Built Environment 16 (2023) 100255. https://doi.org/10.1016/j.dibe.2023.100255.
[35] H.J.B. de Assis, A.C. da Silva Bezerra, J.N. de Paula, W.G. Moravia, Utilization of recycled synthetic fibers in concrete with a focus on structural properties enhancement: a critical literature review, Discov Mater 4 (2024) 77. https://doi.org/10.1007/s43939-024-00150-1.
[36] D. Gao, Y. Tai, L. Yang, Z. Zhang, G. Liu, P. You, Corrosion of Steel Fibers in Chloride-Contaminated Simulated Concrete Pore Solutions, Journal of Materials in Civil Engineering 35 (2023) 04022429. https://doi.org/10.1061/(ASCE)MT.1943-5533.0004591.
[37] Enhancing strength properties of fiber-reinforced concrete using graded alkali-resistant glass fibers | Innovative Infrastructure Solutions, (n.d.). https://link.springer.com/article/10.1007/s41062-025-01923-0 (accessed January 7, 2026).
[38] E. Ozcelikci, E. Ozdogru, M.S. Tugluca, H. Ilcan, M. Sahmaran, Comprehensive investigation of performance of construction and demolition waste based wood fiber reinforced geopolymer composites, Journal of Building Engineering 84 (2024) 108682. https://doi.org/10.1016/j.jobe.2024.108682.
[39] H. Jahangir Qureshi, J. Ahmad, A. Aljabr, N. Garcia-Troncoso, Review on characteristics of concrete reinforced with nylon fiber, Journal of Engineered Fibers and Fabrics 18 (2023) 15589250231189812. https://doi.org/10.1177/15589250231189812.
[40] M. Gorji Azandariani, M. Vajdian, K. Asghari, S. Mehrabi, Mechanical properties of polyolefin and polypropylene fibers-reinforced concrete–

ARTICLE IN PRESS

An experimental study, Composites Part C: Open Access 12 (2023) 100410. https://doi.org/10.1016/j.jcomc.2023.100410.
[41] M.S. Kumar, R. Manju, Investigation of Acrylic Polymer Modified Hybrid Fibre Concrete on Mechanical and Durability Properties, in: M. Alias Yusof, S. Kolathayar, S. Durgadevagi, R. Ramasubramani (Eds.), International Conference on Civil Engineering Innovative Development in Engineering Advances (ICC IDEA - 2025), Volume 4, Springer Nature, Singapore, 2025: pp. 232–243. https://doi.org/10.1007/978-981-95-2266-8_25.
[42] T.V. Muthukumarana, M.A.V.H.M. Arachchi, H.M.C.C. Somarathna, S.N. Raman, A review on the variation of mechanical properties of carbon fibre-reinforced concrete, Construction and Building Materials 366 (2023) 130173. https://doi.org/10.1016/j.conbuildmat.2022.130173.
[43] L. Cheng, S. Chen, F. Chen, C. Wang, Q. Chen, L. Cheng, S. Chen, F. Chen, C. Wang, Q. Chen, Research Progress and Performance Evaluation of Polyvinyl Alcohol Fiber Engineered Cementitious Composites, Sustainability 15 (2023). https://doi.org/10.3390/su151410991.
[44] M.K. Askar, Y.S.S. Al-Kamaki, A. Hassan, M.K. Askar, Y.S.S. Al-Kamaki, A. Hassan, Utilizing Polyethylene Terephthalate PET in Concrete: A Review, Polymers 15 (2023). https://doi.org/10.3390/polym15153320.
[45] M. Ozturk, Exploring the potential of recycled PAN-type fibers as reinforcement in cement-based composites, Journal of Adhesion Science and Technology 39 (2025) 1821–1837. https://doi.org/10.1080/01694243.2025.2472816.
[46] Polyacrylonitrile fiber: composites and applications, in: Synthetic and Mineral Fibers, Their Composites and Applications, Woodhead Publishing, 2024: pp. 269–290. https://doi.org/10.1016/B978-0-443-13623-8.00009-5.
[47] C1437 Standard Test Method for Flow of Hydraulic Cement Mortar, (n.d.). https://store.astm.org/c1437-20.html (accessed January 7, 2026).
[48] C348 Standard Test Method for Flexural Strength of Hydraulic-Cement Mortars, (n.d.). https://store.astm.org/c0348-21.html (accessed January 7, 2026).
[49] Standard Test Method for Compressive Strength of Hydraulic Cement Mortars (Using 2-in. or [50-mm] Cube Specimens), (n.d.). https://store.astm.org/c0109_c0109m-20.html (accessed January 7, 2026).
[50] C642 Standard Test Method for Density, Absorption, and Voids in Hardened Concrete, (n.d.). https://store.astm.org/c0642-21.html (accessed May 20, 2026).
[51] R. Kumar, B. Bhattacharjee, Study on some factors affecting the results in the use of MIP method in concrete research, Cement and Concrete Research 33 (2003) 417–424. https://doi.org/10.1016/S0008-8846(02)00974-2.

ARTICLE IN PRESS

ARTICLE IN PRESS

[52] W. Ma, G. Wang, Y. Zhou, Q. Xu, Y. Dai, Polyacrylonitrile fiber reinforced 3D printed concrete: Effects of fiber length and content, Journal of Building Engineering 97 (2024) 110869. https://doi.org/10.1016/j.jobe.2024.110869.
[53] Z. Luo, X. Zhang, X. Liu, C. Tian, L. Liu, Z. Chen, H. Tan, H. Yang, Effects of styrene-acrylic emulsion on toughness, volume stability and fiber dispersion of hybrid fibers reinforced ultra-high performance geopolymer concrete, Construction and Building Materials 473 (2025) 140930. https://doi.org/10.1016/j.conbuildmat.2025.140930.
[54] L. Wang, T. He, Y. Zhou, S. Tang, J. Tan, Z. Liu, J. Su, The influence of fiber type and length on the cracking resistance, durability and pore structure of face slab concrete, Construction and Building Materials 282 (2021) 122706. https://doi.org/10.1016/j.conbuildmat.2021.122706.
[55] M. Qin, P.L. Li, Z.L. Hong, C. Lian, C. Wang, Q.Q. Zou, B. Fu, Experimental and numerical evaluation of indirect tensile properties of concrete containing macro fibers processed from waste GFRP composites, Case Studies in Construction Materials 24 (2026) e05686. https://doi.org/10.1016/j.cscm.2025.e05686.
[56] C. Ding, L.P. Guo, B. Chen, Theoretical analysis on optimal fiber-matrix interfacial bonding and corresponding fiber rupture effect for high ductility cementitious composites, Construction and Building Materials 223 (2019) 841–851. https://doi.org/10.1016/j.conbuildmat.2019.07.022.
[57] T. Chen, X. Gao, M. Ren, Effects of autoclave curing and fly ash on mechanical properties of ultra-high performance concrete, Construction and Building Materials 158 (2018) 864–872. https://doi.org/10.1016/j.conbuildmat.2017.10.074.
[58] K. Xu, W. Huang, L. Zhang, S. Fu, M. Chen, S. Ding, B. Han, Mechanical properties of low-carbon ultrahigh-performance concrete with ceramic tile waste powder, Construction and Building Materials 287 (2021) 123036. https://doi.org/10.1016/j.conbuildmat.2021.123036.
[59] L. Zhang, B. Liu, M. Guo, X. Zhan, K. Xu, H. Li, Y. Wang, X. Wang, B. Han, Ultra-high performance concrete with excellent high-temperature resistance by using waste ceramic fine aggregates, Structures 82 (2025) 110548. https://doi.org/10.1016/j.istruc.2025.110548.

ARTICLE IN PRESS